Epigenetic Landscape Analysis of the Long Non-Coding RNA and Messenger RNA in a Mouse Model of Corneal Alkali Burns

Li Jiang,[1] Wenjing He,[1] Fen Tang,[1] Ningning Tang,[1] Guangyi Huang,[1] Wei Huang,[1] Xiaonian Wu,[1] Jianpei Guan,[1] Siming Zeng,[1] Min Li,[1] Qi Chen,[1] Mingyuan Zhang,[2] Haibin Zhong,[1] Qianqian Lan,[1] Ling Cui,[1] Lili Li,[1] and Fan Xu[1]

[1]Department of Ophthalmology, People's Hospital of Guangxi Zhuang Autonomous Region, Nanning, Guangxi, People's Republic of China
[2]Laboratory Animal Center, Guangxi Medical University, Nanning, China

Correspondence: Ling Cui, Lili Li, and Fan Xu, Department of Ophthalmology, People's Hospital of Guangxi Zhuang Autonomous Region, No. 6, Taoyuan Road, Nanning 530021, Guangxi, People's Republic of China;
eyecuil@163.com;
hmily-lily@163.com;
oph_fan@163.com.

LJ, WH, FT, and NT contributed equally to this work.

Received: July 13, 2020
Accepted: January 20, 2021
Published: April 23, 2021

Citation: Jiang L, He W, Tang F, et al. Epigenetic landscape analysis of the long non-coding RNA and messenger RNA in a mouse model of corneal alkali burns. *Invest Ophthalmol Vis Sci.* 2021;62(4):28. https://doi.org/10.1167/iovs.62.4.28

Purpose. Corneal alkali burns (CABs) are a common clinical ocular disease, presenting a poor prognosis. Although some long noncoding RNAs (lncRNAs) reportedly play a key role in epigenetic regulation associated with CABs, studies regarding the lncRNA signature in CABs remain rare and elusive.

Methods. A CAB model was established in C57BL/6J mice and profiling of lncRNA expressions was performed by RNA-Seq. Gene ontology (GO) and Kyoto Encyclopedia of Genes and Genomes (KEGG) enrichment analyses were conducted to predicate the related pathological pathways and candidate genes. RT-qPCR was used to verify the expression pattern of lncRNAs and related mRNAs, both in vitro and in vivo. Data were statistically analyzed by GraphPad Prism version 6.0.

Results. In all, 4436 aberrantly expressed lncRNAs were identified in CAB mice when compared with control mice. In the top 13 aberrantly expressed lncRNAs, Bc037156 and 4930511E03Rik were confirmed as the most significantly altered lncRNAs. Pathway analysis revealed that mitogen-activated protein kinase (MAPK) signaling pathway was most enriched. Following 4930511E03Rik siRNA treated, Srgn, IL-1β and Cxcr2 were significant upregulated in corneal epithelial cells, corneal keratocytes, and bone marrow dendritic cells, with NaOH treatment. Moreover, after Bc037156 siRNA treated, expression levels of IL-1β and Srgn were significantly downregulated in the three cell lines.

Conclusions. Our study suggests that Bc037156 and 4930511E03Rik may be involved in inflammation, immune response, and neovascularization by regulating Srgn, IL-1β, and Cxcr2 expression after CAB. These candidate lncRNAs and mRNAs may be the potential targets for the treatment strategy of the alkali injured cornea.

Keywords: long non-coding RNAs (lncRNAs), corneal alkali burn (CAB), immune response, neovascularization, inflammation

Corneal alkali burns (CABs) are a common ophthalmic emergency.[1] Alkali materials damage the ocular surface epithelial cells and infiltrate to the stroma. Then dendritic cells (DCs) migrate into the corneal center in response to inflammation and immune reaction, resulting in severe complications, such as opacity, neovascularization, perforation, decreased visual acuity, and even blindness.[2,3] Corneal neovascularization (CNV) leads to persistent inflammation, scar formation, and it is a high risk factor for corneal allograft rejection.[4,5] The current treatment for inflammation and CNV after CAB include topical steroid application, ascorbic acid, artificial tears, and corneal transplantation.[6,7] Unfortunately, the currently available therapeutic strategies are limited, and, therefore, the precise molecular mechanisms of inflammation and CNV after alkali burns need to be comprehensively elucidated.

Long non-coding RNAs (lncRNAs) refer to heterogeneous transcripts longer than 200 nucleotides, which regulate gene expression via diverse mechanisms and are involved in protein translation, messenger RNA (mRNA) decay, and post-transcriptional processes.[8] Mammalian genomes encode more lncRNAs than any other types of noncoding RNAs, and the identification of functional lncRNAs involved in biological processes is progressively increasing.[9] Recently, studies proved that several common lncRNAs play important roles in biological processes, such as inflammatory response, cell proliferation and migration, and neovascularization by acting as a molecular sponge.[10,11] Furthermore, a growing number of studies revealed that some lncRNAs participate in the pathogenesis of multiple diseases, including cancer, cardiovascular disease, diabetes, and ocular alkali burns by regulating mRNA directly or indirectly.[12–15] In addition,

lncRNAs have been determined as a potential diagnostic or prognostic biomarkers in diseases progression.[14,16] However, a limited number of studies have described the function and regulatory mechanism to a CAB. The role of lncRNAs in the pathogenesis of a CAB remains largely unclear.

In the current study, whole-transcriptome sequencing was used to identify differentially expressed corneal lncRNAs and mRNAs in a CAB model and normal mice. Herein, we aimed to illustrate the comprehensive landscape of lncRNAs following a CAB. Furthermore, we explored the potentially regulated lncRNAs and mRNAs involved in inflammation and CNV after a CAB, identifying a novel target for early therapy.

Materials and Methods

Animals

Sixty female 6 to 8-week-old C57BL/6J mice, weighing 20 to 25 g (provided by Guangxi Animal Experiment Center), were randomly divided into 3 groups (triplicate), each group containing 20 mice. The mice were supplied by Laboratory Animal Center of Guangxi Medical University and maintained under a 12/12 hour light/dark schedule, at approximately 23°C, and 60% humidity, with adequate rodent chow and water available. All animals received humane care in accordance with Association for Research in Vision and Ophthalmology (ARVO) Statement for the Use of Animals in Ophthalmic and Vision Research, and experimental protocols were approved by the Ethics Committee of the People's Hospital of Guangxi Zhuang Autonomous Region and the Institutional Animal Care and Use Committee.

CAB Mouse Model

The CAB model was developed based on a previously described study, with midifications.[1] Briefly, mice were anesthetized using an intraperitoneal injection of 1.5% pentobarbital sodium (35–40 mg/kg). In addition, proparacaine hydrochloride eyedrop (Alkaline; Alcon, Belgium) was used for topical anesthesia. After exposing the eyeball, a filter paper (1.5 mm diameter), immersed in 2 µL 1N NaOH solution, was placed in the center of the right cornea for 50 seconds. After removing the filter paper, the eye was immediately rinsed with sterile saline until pH 7, and antibiotic ointment was applied. The left eyes were maintained as untreated internal controls. After the establishment of the animal model, the mice received levofloxacin eye drops (Cravit; Santen, China), thrice daily for 3 days.

Cell Cultures

Primary corneal epithelial cells (CECs) and corneal keratocytes (CKs) were isolated from normal cornea of C57BL/6J mice, as previously described with some modifications.[17] Shortly, the cornea was cut and washed thrice with phosphate-buffered saline containing 5% penicillin/streptomycin (Gibco, Carlsbad, CA, USA). Subsequently, the epithelial layer of the limbal region contain progenitor cells was gently peeled off under the microscope using a cell scraper, then trypsinized with 0.25% trypsin without ethylenediaminetetraacetic acid (EDTA) for 20 minutes. After neutralized in Dulbecco's modified Eagle's medium (DMEM; Invitrogen, Carlsbad, CA, USA) with 5% fetal bovine serum (FBS; Gibco, Carlsbad, CA, USA), cells were centrifuged and seeded in complete medium composed of DMEM, 10% FBS, 5 ng/mL epidermal growth factor (EGF; Peprotech, Cranbury, NJ, USA), and 1% penicillin/streptomycin. Next, the corneal epithelial and endothelial sheets were both removed, and the stroma was obtained. The remaining corneal stromal layer was minced and incubated with 2 mg/mL collagenase (Sigma, Gaithersburg, MD, USA), and diluted in DMEM overnight at 37°C. Then, the samples were centrifuged and resuspended in complete medium contained DMEM, 10% FBS, 2 mM L-glutamine, and 1% penicillin/streptomycin.

Bone marrow dendritic cells (BMDCs) were generated from C57BL/6J mice as previously described.[18] In brief, bone marrows from the femurs were flushed, and red blood cells were lysed in Ammonium-chloride-potassium (ACK) lysing buffer for 2 minutes. Then, bone marrow cells were filtered through a 200 µm cell strainer. The remaining samples were centrifuged, and the supernatant were discarded. Later, the cells were resuspended in Roswell Park Memorial Institute (RPMI) 1640 (Invitrogen) medium supplemented with 10% FBS, 20 ng/mL granulocyte-macrophage colony-stimulating factor (GM-CSF; Peprotech), 10 ng/mL interleukin-4 (IL-4; Peprotech), 2 mM L-glutamine (Peprotech), and 1% penicillin/streptomycin.

Cell Treatment and Transfection

On reaching 85% confluency, the cells were passaged 1:3. Then, P3 generation cells were treated with 0.5 mol/L NaOH to establish an alkali-burn model in the 3 different cell lines. Subsequently, the cells were transfected with the constructed siRNAs (10 nM) specific for 4930511E03Rik and Bc037156 (IGEbio, Guangzhou, China), or their corresponding negative controls using the Lipofectamine RNAiMax kit (Invitrogen), in accordance with the manufacturer's instructions. The siRNA sequences are shown in Supplementary Table S1.

Total RNA Extraction and RNA Sequencing

After 7 days, the mice were euthanized by an overdose of ketamine, and the cornea was cut off for subsequent experiments. TRIzol reagent (Invitrogen) was used for RNA extraction according to the manufacturer's instructions. For RNA-sequencing (RNA-Seq), RNA was quantified with a NanoPhotometer (Implen Inc., Westlake Village, CA, USA), and RNA Integrity Number (RIN) was assessed using the Agilent 2100 RNA Nano 6000 Assay Kit (Agilent Technologies, Santa Clara, CA, USA). RIN value of ≥8 was considered high quality and was acceptable. In brief, the libraries were constructed according to the manufacturer's guide of NEB Next Ultra Directional RNA LibraryPrep Kit for Illumina (NEB, Ipswich, MA, USA). First, rRNAs were extracted from the total RNA with Ribo-Zero Gold Kits (NEB). A fragmentation buffer was added to fragment the RNA. Then the RNA fragments were used as the templates to synthesize cDNA with random hexamers. The double-stranded cDNA products were amplified and purified to prepare the libraries. Next, the libraries were sequenced using the Illumina MiSeq platform with MiSeq Reagent Kit version 3 (Illumina Inc., San Diego, CA, USA). We have submitted the transcriptome dataset to SRA. The SRA sample IDs are SRR13449163, SRR13449162, SRR13449161, SRR13449160, SRR13449159, and SRR13449158.

Investigative Ophthalmology & Visual Science

Prediction of lncRNA

The original RNA-seq were transformed into raw reads using the bcl2fastq2 software. Subsequently, raw reads were filtered to remove low-quality reads (bases qualify ≤19), Ns reads, raw Q30 bases, rRNA mapping reads, and adapter polluted reads. Then, the remaining clean reads of all samples were aligned to the reference genome mainly using the Hierarchical Graph FM index (HGFM) with HiSAT2.[19] The StringTie's network flow algorithm[19] was used to accurately reconstruct transcripts. For lncRNAs profiling, a transcription length of ≥200 bp and exons ≥2 were selected. Then, the following prediction methods were utilized: Coding-Non-Coding Index (CNCI), Coding Potential Calculator (CPC), pfamscan,[20] and Coding Potential Assessment Tool (CPAT) prediction. A CPC score <0 and CNCI score <0 were selected, with protein families (Pfams) significantly higher than other transcripts and Fickett and Hexamer scores of CPAT as potential lncRNAs. The intersection of performed predictions indicated the potential lncRNAs, which was displayed as Venn diagrams. To normalize gene expression, fragments per kilobase of exon per million reads mapped (FPKM)[21] were determined. Furthermore, the DEGSeq[22] package was used to determine the differential expressed genes. The false-discovery rate (FDR) was used to determine the significance threshold of the *P* values for multiple tests. If the |log2Ratio| was ≥1 and *Q*-value <0.05, the genes were selected. The heatmap presents the significant differentially expressed lncRNAs.

$$FPKM = \frac{10^3 * F}{NL/10^6}$$

Gene Ontology and Kyoto Encyclopedia of Genes and Genomes Pathway Analyses

To analyze the potential functions of significant differentially expressed genes, Gene Ontology (GO) enrichment analysis (http://amigo.geneontology.org/amigo) was performed in molecular function (MF), cellular component (CC), and biological process (BP), using the "clusterProfiler" package. GO terms with *P* values < 0.05 were identified significantly enriched. Additionally, the Kyoto Encyclopedia of Genes and Genomes (KEGG) database (https://www.genome.jp/kegg/) was used to analyze the pathway among these candidate genes. To visualize the pathway relationships with a high coefficient, a hypergeometric distribution analysis was performed to identify GO annotation and KEGG pathway enrichment coding genes.

Construction of the lncRNA-mRNA Co-Expression Network

Trans-regulation and *cis*-regulation were used to predict potential genes. The mRNAs were identified as potential target genes when loci were ranged 100 kb upstream and downstream of the specified lncRNAs. Next, we constructed a co-expression network, as shown in Figure 6 A, to determine the relationship between the candidate lncRNAs and regulated mRNAs. Pearson's correlation co-efficient was calculated, and the R-value was used to compare the correlation co-efficient of expression levels between differentially expressed lncRNAs and mRNAs. If the *P* value was less than 0.001, we considered this lncRNA-mRNA pair to be linearly correlated. Finally, we selected the most significantly upregulated and downregulated lncRNAs and target mRNAs to visually represent a lncRNA-mRNA co-expression network via Cytoscape (http://www.cytoscape.org).

Real-Time Quantitative Polymerase Chain Reaction

To verify the significantly differentially expressed lncRNAs and potential target mRNAs expression, RT-qPCR was performed using different corneal samples and cells. Expression levels were measured using the Platinum SYBR Green qPCR SuperMix-UDG with ROX kit (Invitrogen), in accordance with the manufacturer's standard instruction and the primers listed in Table 1. Relative gene expression levels were normalized to GAPDH (housekeeping gene). The following conditions were used as cycle parameters: 50°C for 2 minutes (UDG incubation), 95°C for 2 minutes, 40 cycles of: 95°C for 15 seconds and 60°C for 30 seconds. The relative expression of the chosen transcripts was quantified using the $2(-\Delta\Delta Ct)$ method and experiments were performed in triplicate. Primers were designed by NCBI's Primer blast3 and Origene.

Statistical Analysis

All data were analyzed using GraphPad Prism version 6.0 (GraphPad Software Inc., San Diego, CA, USA). The distribution of characteristics between two groups of variances were determined by Student *t*-test. The data were presented as mean ± standard error of the mean (SEM). The *P* values < 0.05 were considered statistically significant.

Results

Expression Profiling of lncRNAs in the Mouse CAB Model

Seven days after NaOH injury, CNV was found to originate from the limbal vessels, extending to the central of the cornea (Fig. 1B). An obvious inflammatory response presenting corneal edema and opacity was observed. Moreover, epithelial lesions were detected using a fluorescence sodium dye (Fig. 1C). We then performed RNA-Seq to identify lncRNAs linked to the cornea following NaOH injury. Six RNA-Seq libraries were constructed, and duplicate samples were obtained. The lncRNAs were longer than 200 bp, with more than 2 exons (Figs. 1D, 1E). Subsequently, a heatmap cluster of Pearson correlation coefficients demonstrated the reproducibility of biological and sequencing technical replicates (Fig. 1F). The Venn diagram presents the intersection of four computational approaches (CPC/CNCI/PFAM/CPAT) for candidate lncRNA from putative protein-coding RNAs, and 10,706 lncRNAs were predicted as potential lncRNAs (Fig. 1G).

Identification of the Significant Differentially Expressed lncRNAs and mRNAs after a CAB

DEGseq were performed for differential expression analysis. Genes with a *Q*-value < 0.05 and |log2Ratio| ≥1 were identified as differentially expressed genes. In total, 14,464 differentially expressed lncRNAs were identified in the 3 groups. The histograms present aberrantly expressed

Investigative Ophthalmology & Visual Science

Table 1. Primers for Identifying Genes (Including 13 Dysregulated lncRNAs and 13 Dysregulated mRNAs)

Gene	Forward Primer	Reverse Primer
GAPDH	CATCACTGCCACCCAGAAGACTG	ATGCCAGTGAGCTTCCCGTTCAG
Neat1	TGTATTGCCTCTGCCTGTGG	GGCAACAAAAGCAAACGCAC
H19	AGAGTGGCTCTGGCAAAGTC	TCTGCTGGAGACCTGGCTAT
2310001H17Rik	CAGGATGACTTAGTGTCCCACTA	GTATGTTCTGGGAAAGGAACTGG
Gm38171	AGACAGCTGTTTTCATGTGGC	ACCGTTCAAGTCCAGGACGAT
Gm29113	CTTTCTGAGCCGATAAATCCCA	GAAGGAAGGGTATATGAGTTTGCC
Bc037156	GAAAACTCTTCTCCTGCTCGC	CCGTATGGGGGAAAGGGAATC
Ac160051.2	TCCAGCTAATGCCAGGTAACA	CATCTCACGGCCTCCCATTC
Ac118476.6	GATGAAACCCCGGTCCACAT	GAGCCTAGAGTCGGGGCTAT
Gm16025	CCTCCCTCTACCTCTGGCTT	AAGGGTCATCGGTCTAGGCT
Gm38348	GCCTGGGTGGTGTACATTGA	GGATGAGAGACCCCAGTCCT
Gm37107	CTGTTCTACACATTCTGCTGGAG	CTTAGGGTCACTCAGAGACATGA
Gm11611	CTCCCTTCCTTGTGTGATTCTTC	GTAAGGAGCAGCATATGACTCAC
4930511E03Rik	CTTCAGTGGCCACCCGTAAT	CCTGAGCCTACTGGGTCTCT
Slurp1	GTGCAAGATGGAAGACACAGCC	AGACAGGATGGGCAACGCCAAT
Lypd2	TCCAACTGTGTCACCACCAC	CACATCCGAAGGCTCACACT
Ppbp	CTGATCCTTGTTGCGCTGGCTC	GCCTGTACACATTCACAAGGGAG
Sell	TTCCTGTAGCCGTCATGGTC	TCCATCCTTTCTTGAGATTTCTTGC
Cxcl5	CGGTTCCATCTCGCCATTCA	GCTATGACTGAGGAAGGGGC
Npy	TACTCCGCTCTGCGACACTACA	GGCGTTTTCTGTGCTTTCCTTCA
Cxcr2	CTCTATTCTGCCAGATGCTGTCC	ACAAGGCTCAGCAGAGTCACCA
Krt12	CGAGAGTGGTATGAAACACGGAG	CGTTGCTGACTCTGGCAGAAAC
Erich5	CCAGCCGAAACTGGAGAGACAG	GCTTCCACCTTTTCTCCTGTCTC
Ppp1r3c	TGCTTGGCTCATTCACCACCTC	CACTCTGCGATTTGGCTTCCTG
IL-1β	TGGACCTTCCAGGATGAGGACA	GTTCATCTCGGAGCCTGTAGTG
Srgn	TGCGAACTGCATCGAGGAGAAG	CCCGAACCTGACCCATAGTCAT
Rascrf1	AAGGTCACCGTGCCTCAGATGA	ACGCTGGCATAGCGGATCTGAA

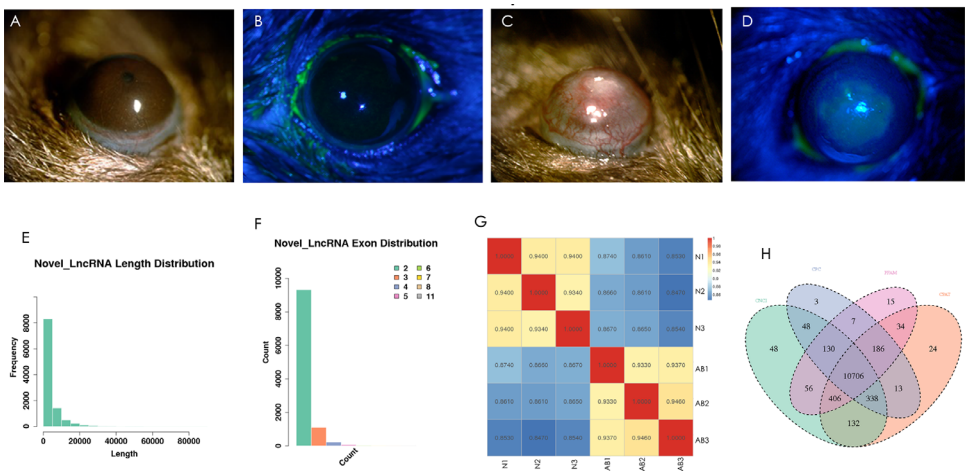

Figure 1. Identification of related lncRNAs in the CAB model. (**A**) Representative slit-lamp biomicroscopic images from normal mice. (**B**) Representative slit-lamp biomicroscopic images of the normal cornea with fluorescein sodium staining. (**C**) Representative slit-lamp biomicroscopic images on day 7 after a CAB. (**D**) Representative images of fluorescence sodium staining on day 7 after a CAB. (**E**) Histogram presenting length distribution of novel lncRNA. (**F**) Histogram presenting the number of novel lncRNA. (**G**) Heatmap of gene expression correlation, the numerical value refers to the correlation coefficient. (**H**) Venn diagram presents overlapping potential lncRNAs of four computational approaches (CPC/CNCI/PFAM/CPAT). CAB, corneal alkali burns; lncRNAs, long noncoding RNAs; AB, alkali burn.

lncRNAs, mRNAs, and total RNA numbers in each group of CAB mice compared with their age-matched normal controls (Figs. 2A–C). Moreover, the Volcano plot revealed the different lncRNA expression profiles in each group (Figs. 2D–F). The heatmap of hierarchical clustering revealed that the lncRNA and mRNA expression patterns among samples were distinct (Figs. 2G, 2H). Furthermore, a Venn diagram was used to analyze the changes in lncRNAs, with 4436 aberrantly expressed lncRNAs (3147 known and 1289 new) identified (Fig. 2I).

Table 2 and Table 3 present the top 13 dysregulated known lncRNAs and mRNA, respectively. The top 13 dysregulated novel lncRNAs are list in Supplementary Table S2. We verified the expression of these select genes by RT-qPCR in three duplicate samples. The results showed that Neat1, H19, 2310001H17Rik, Gm29113, Bc037156, and Ac118476.6

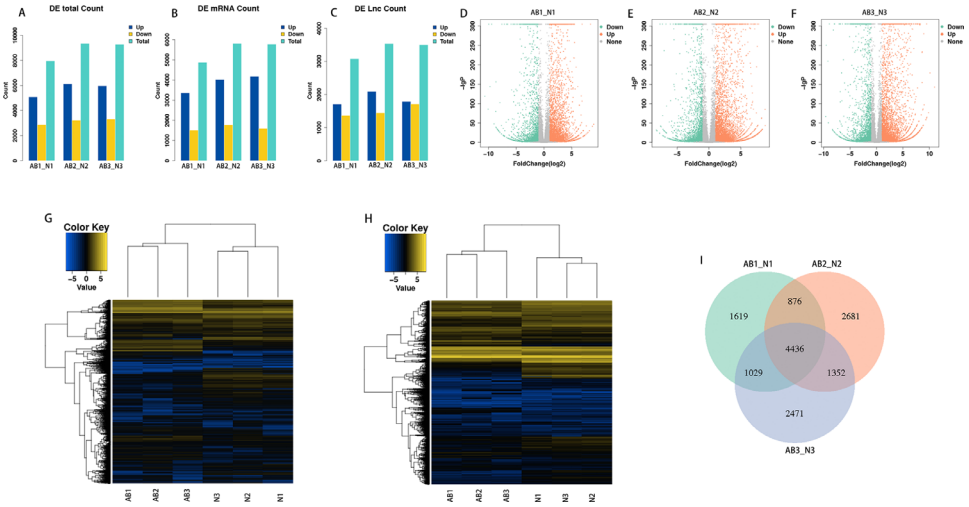

Figure 2. Identification of the significant differentially expressed lncRNAs and mRNAs. (**A**) Comparing the sum count of differentially expressed lncRNA and mRNA in the three groups. (**B, C**) Comparison of the number of differentially expressed lncRNA **B** and mRNA **C**. (**D–F**) Volcano plot of the different lncRNA expression profiles in each group. (**G, H**) Heatmap of hierarchical clustering of lncRNA **G** and mRNA **H** expression patterns among samples. (**I**) Venn diagram of aberrantly expressed lncRNAs. CAB, corneal alkali burns; lncRNAs, long noncoding RNAs; AB, alkali burn.

Table 2. The List of the Top 13 Dysregulated Known Lncrnas

Gene	Gene Name	Biotype	Regulation	Log2 Fold Change	FDR Value	Locus
ENSMUSG00000087042	Neat1	lincRNA	Up	1.0418163	1.53E-95	chr19:5824708-5845478:-
ENSMUSG00000000031	H19	lincRNA	Up	2.859068166	7.92E-76	chr7:142575529-142578143:-
ENSMUSG00000097354	2310001H17Rik	lincRNA	Up	1.813001523	8.38E-63	chr6:129208412-129238725:-
ENSMUSG00000102196	Gm38171	lincRNA	Up	7.075608527	1.39E-61	chr2:11315372-11319874:-
ENSMUSG00000100354	Gm29113	lincRNA	Up	1.310736936	6.50E-58	chr1:69490357-69493788:-
ENSMUSG00000105888	Bc037156	lincRNA	Up	5.831682944	4.86E-56	chr5:87908779-87914171:+
ENSMUSG00000111167	Ac160051.2	lincRNA	Up	5.522354886	4.25E-45	chr9:42141993-42146506:+
ENSMUSG00000111720	Ac118476.6	lincRNA	Up	6.320721025	1.24E-39	chr9:120834363-120844936+
ENSMUSG00000089652	Gm16025	lincRNA	Down	-3.56006368	2.93E-180	chr1:85326729-85342615:+
ENSMUSG00000102357	Gm38348	sense_intronic	Down	-4.711405755	8.40E-102	chr2:4217081-4219353:+
ENSMUSG00000102136	Gm37107	sense_intronic	Down	-4.377073972	9.96E-97	chr2:4178110-4180661:+
ENSMUSG00000087042	Gm11611	sense_intronic	Down	-2.027108934	7.25E-61	chr11:97519612-97521895:-
ENSMUSG00000108187	4930511E03Rik	lincRNA	Down	-5.130490087	1.93E-48	chr6:94943834-94951545:+

Table 3. The List of the Top 13 Dysregulated mRNAs

Gene	Gene Name	Regulation	Log2 Fold Change	FDR Values	Related With the Candidate lncRNA	Locus
ENSMUSG00000022596	Slurp1	Down	−9.939610494	0	–	chr15:74724318-74728034:-
ENSMUSG00000022595	Lypd2	Down	−9.422862851	0	–	chr15:74732247-74734329:-
ENSMUSG00000029819	Npy	Down	−7.570429779	0	–	chr6:49822710-49829507:+
ENSMUSG00000020912	Krt12	Down	−6.754788086	0	–	chr11:99415666-99422259:-
ENSMUSG00000044726	Erich5	Down	−4.389439667	0	–	chr15:34453312-34473892:+
ENSMUSG00000067279	Ppp1r3c	Down	−7.138198182	0	–	hr19:36731737-36736653:-
ENSMUSG00000032356	Rasgrf1	Down	−5.925387838	0	ENSMUSG00000000031	chr9:89909908-90026977:+
ENSMUSG00000029372	Ppbp	Up	8.384511557	0	ENSMUSG00000111720	chr5:90768518-90770063:+
ENSMUSG00000026581	Sell	Up	5.401482037	0	ENSMUSG00000111167	chr1:164061982-164084181:+
ENSMUSG00000020077	Srgn	Up	5.08293694	0	ENSMUSG00000105888 ENSMUSG00000108187	chr10:6249383362527451:-
ENSMUSG00000027398	IL-1β	Up	5.190080668	0	ENSMUSG00000105888 ENSMUSG00000108187	ch2:129364570-129371139:-
ENSMUSG00000026180	Cxcr2	Up	5.359540274	0	ENSMUSG00000105888 ENSMUSG00000108187	chr1:7415398974161246:+
ENSMUSG00000029371	Cxcl5	Up	6.870698167	0	–	chr5:90759360-90761624:+

Investigative Ophthalmology & Visual Science

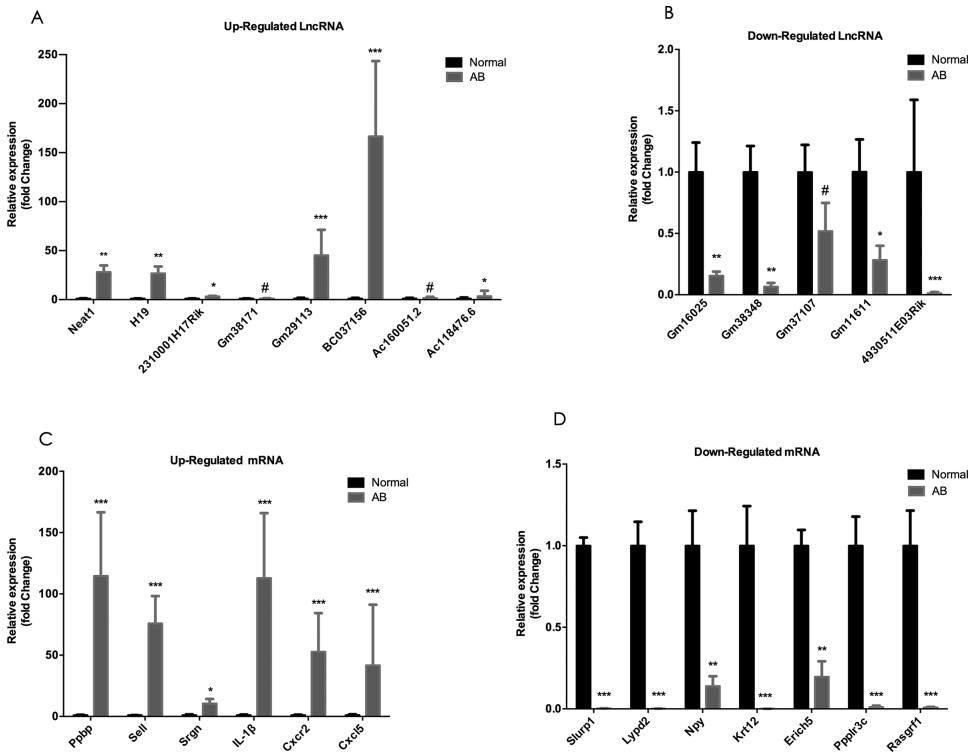

Figure 3. Validation of expression profiles of lncRNAs and mRNAs via RT-qPCR. (**A, B**) Expression levels of top eight upregulated and top five downregulated lncRNAs in the cornea after alkali burn. (**C, D**) The expression levels of top six upregulated and top seven mRNAs in the cornea after alkali burn, respectively. Experiments were performed in triplicate. AB, alkali burn. #: $P > 0.05$, *: $P < 0.05$, **: $P < 0.01$, ***: $P < 0.001$. CAB, corneal alkali burns; lncRNAs, long noncoding RNAs; RT-PCR, reverse transcription-polymerase chain reaction.

were significantly increased following CAB injury (Fig. 3A). Among them, Bc037156 was the most significantly upregulated. In addition, Gm16025, Gm38348, Gm11611, and 4930511E03Rik were significantly downregulated, with 4930511E03Rik most significantly downregulated (Fig. 3B). Next, we verified the top 13 dysregulated mRNAs expression level, revealing significantly altered expression levels of chosen mRNAs. Among them, expression levels of Ppbp (Pro-platelet basic protein), Sell (selectin L), Srgn (serglycin), IL-1β, Cxcr2 (CXC chemokine receptor 2), and Cxcl5 (C-X-C motif chemokine 5) were significantly elevated (Fig. 3C), whereas those of Slurp1 (secreted Ly6/uPAR-related protein-1), Lypd2 (LY6/PLAUR domain category 2), Npy (neuropeptide Y), Krt12 (Keratin 12), Erich5 (glutamate rich 5), Ppp1r3c (protein phosphatase 1), and Rasgrf1 (Ras-specific guanine nucleotide-releasing factor 1) were reduced (Fig. 3D). The above-mentioned genes may be potential regulatory genes associated with CAB injury.

Bioinformatic Functional Analysis of Differentially Expressed lncRNAs

To further analyze the function of differentially expressed lncRNAs and the potential target mRNAs among samples, GO enrichment analyses were performed. If the Jensen–Shannon (JS) score >0.5, the significantly altered lncRNAs and mRNAs were selected. The expression levels of the remaining tissue-specific lncRNAs (Fig. 4A) and mRNAs (Fig. 4B) were illustrated in a heatmap. To identify potential protein-coding genes proximal to tissue-specific lncRNAs, we performed *cis* and *trans* analyses for all aberrantly expressed known lncRNAs. Subsequently, GO annotation was utilized to investigate the function of differentially expressed lncRNAs, enumerating the number in GO terms. In BP, CC, and MF, the numbers of differentially expressed lncRNAs in cell process and biological regulation, cell part and organelle, catalytic activity, and binding were the highest (Fig. 4F). To decipher biological processes involved in response to the microenvironment, GO enrichment of DEGseq was applied with $q < 0.05$, which was considered to be significantly enriched. As shown in Figures 4C to E, differentially expressed lncRNAs were significantly enriched in AMPA glutamate receptor, B cell activation and differentiation, and 1-acylglycerol-3-phosphate O-acyltransferase activity. These results indicated that the differentially expressed lncRNA-mRNA interaction pairs may participate in pathological changes observed after CAB injury.

KEGG Pathway Analysis of Differentially Expressed lncRNAs

The KEGG pathway analysis demonstrated that the genes were enriched in multiple pathways (Fig. 5A), among them, the MAPK (mitogen-activated protein kinase) signaling pathway was the most enriched (Fig. 5B). Furthermore, the vascular endothelial growth factor (VEGF) signaling pathway, tumor necrosis factor (TNF) signaling pathway (Fig. 5C), Th1 and Th2 cell differentiation, Th17 cell differentiation, T cell receptor signaling pathway, PI3K-Akt signaling pathway, cytokine-cytokine receptor interaction, and the

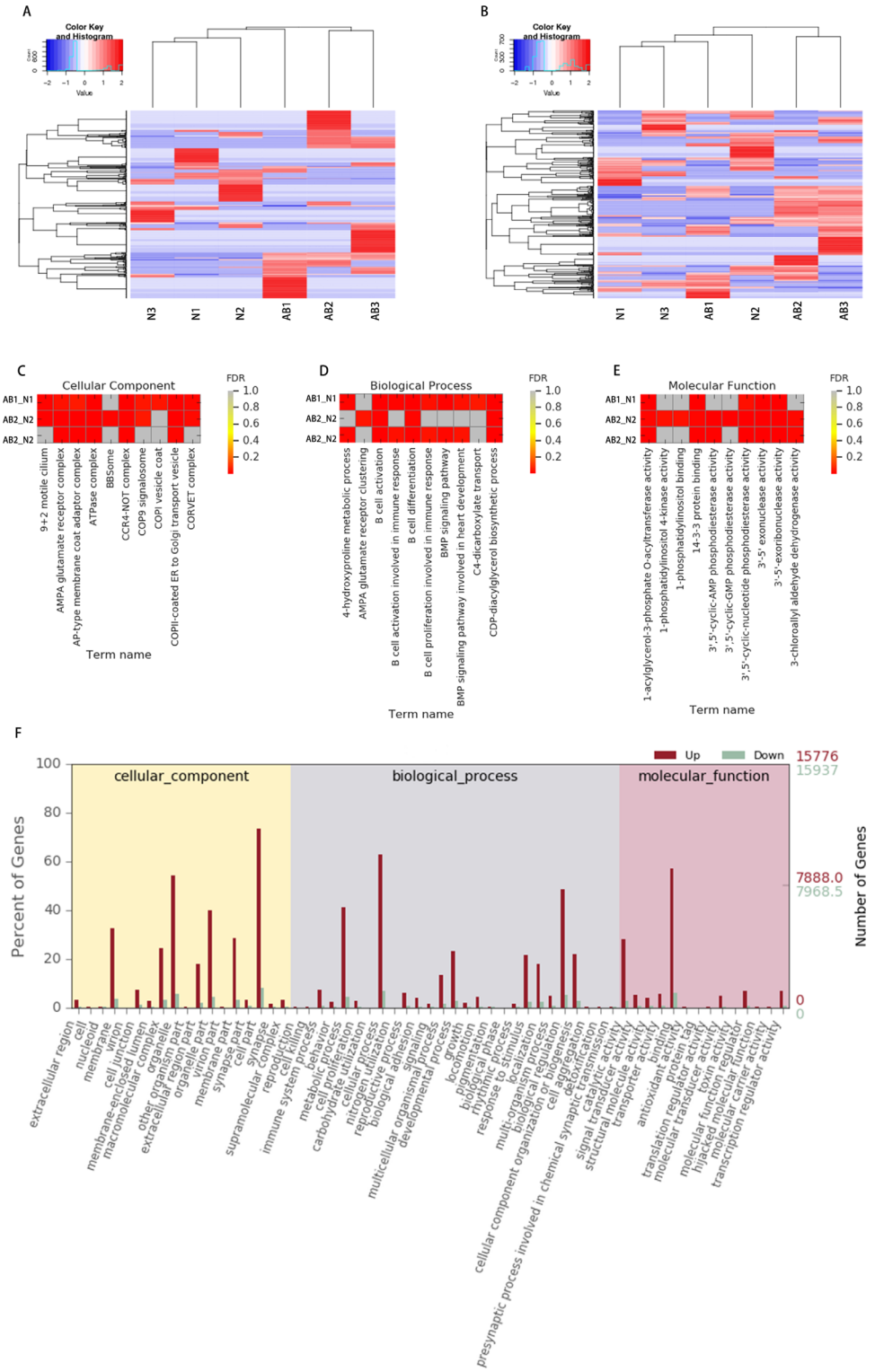

Figure 4. Bioinformatic functional analysis of differentially expressed lncRNAs. (**A, B**) Heatmap of expression levels of tissue-specific lncRNAs **A** and mRNAs **B**. (**C–E**) GO enrichment of DEGseq shows that differentially expressed lncRNAs enriched in CC **C**, BP **D**, and MF **E**. (**F**) The number of differentially expressed lncRNAs in CC, BP, and MF. lncRNAs, long noncoding RNAs; GO, Gene Ontology; CC, cellular component; MF, molecular function; BP, biological process.

Investigative Ophthalmology & Visual Science

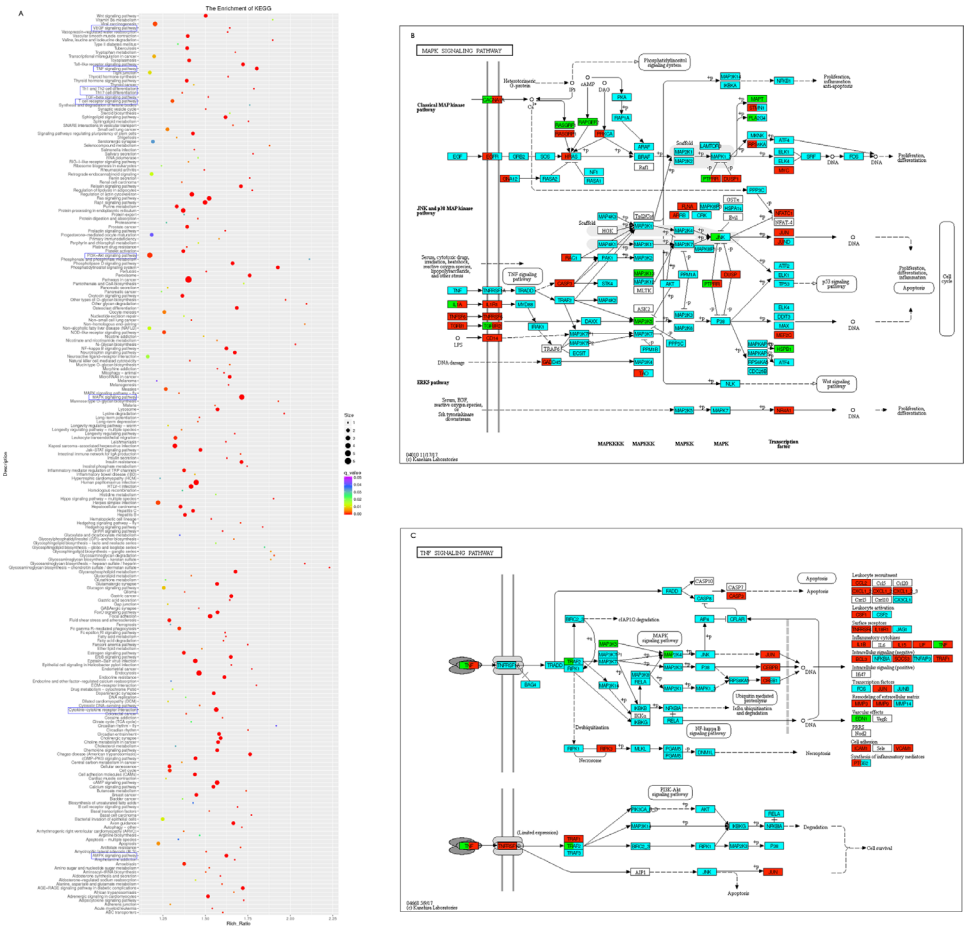

Figure 5. Signaling pathway analysis of differentially expressed lncRNAs. (**A**) The KEGG pathway analysis demonstrates that the genes are enriched in multiply pathways. (**B**) MAPK signaling pathway map. (**C**) TNF signaling pathway map. Dot size **A** indicates the gene numbers enriched in this pathway. Red **B** and **C** indicates upregulated genes. *Green* **B** and **C** indicates downregulated genes. lncRNAs, long noncoding RNAs; KEGG, Kyoto Encyclopedia of Genes and Genomes; MAPK, mitogen-activated protein kinase; TNF, tumor necrosis factor.

AMPK (5' AMP-activated protein kinase) signaling pathway closely correlated with pathological changes in the CAB model.

lncRNA/mRNA Co-Expression Network and Validation of Regulated mRNAs

Based on the above results, Bc037156 and 4930511E03Rik were the most significantly altered lncRNAs and may play a critical role in the molecular network of CAB. Figure 6A shows the co-expression network of Bc037156 and 4930511E03Rik and target mRNAs. For further corroboration, we compared the expression levels of the two lncRNAs in CEC, CK, and BMDC. These three types of cells are commonly present in the cornea and may play key roles in pathological changes following a CAB. Consistent with the qRT-PCR results in the cornea, Bc037156 was significantly increased after NaOH treatment in all three cell types (Fig. 6B). Moreover, 4930511E03Rik was significantly reduced (Fig. 6C).

By performing an lncRNA-mRNA co-expression network analysis, we observed that Bc037156 and 4930511E03Rik both regulated the genes Srgn, IL-1β, and Cxcr2. To verify the regulatory mechanism, knockdown of the two lncRNAs was performed in vivo. As shown in Figures 6D to I, the expression levels of IL-1β, Cxcr2, and Srgn were significantly elevated following 4930511E03Rik knockdown in all 3 cell lines. IL-1β and Srgn were significantly reduced in the three cells treated with si-Bc037156. Besides, Cxcr2 expression was significantly reduced in CEC and CK, but not in BMDCs. These results were consistent with the RNA-Seq profiling.

Discussion

Chemical injury, especially alkali injury, is one of the most devastating injuries to the cornea. Persistent inflammation releases inflammatory factors, which are recognized and processed by antigens present cells (APCs), affecting the balance of Th1/Th2, Th17 cells secrete cytokines to regulate Th1 cells, which led to induces of the immune cells activation.[23,24] During inflammation, activated immune cells produce angiogenic factors and promote aberrant CNV. Simultaneously, neovascularization will aggravate inflammation and immune reaction.[25,26] Additionally, the process of epithelial wound healing is the decisive factor for injured tissue. Current studies reported that controlling inflammation, promoting wound healing, reducing CNV, and regulating immune cells are the key strategies for the treatment of CAB.[7,27,28] However, the molecular mechanism underlying a

Investigative Ophthalmology & Visual Science

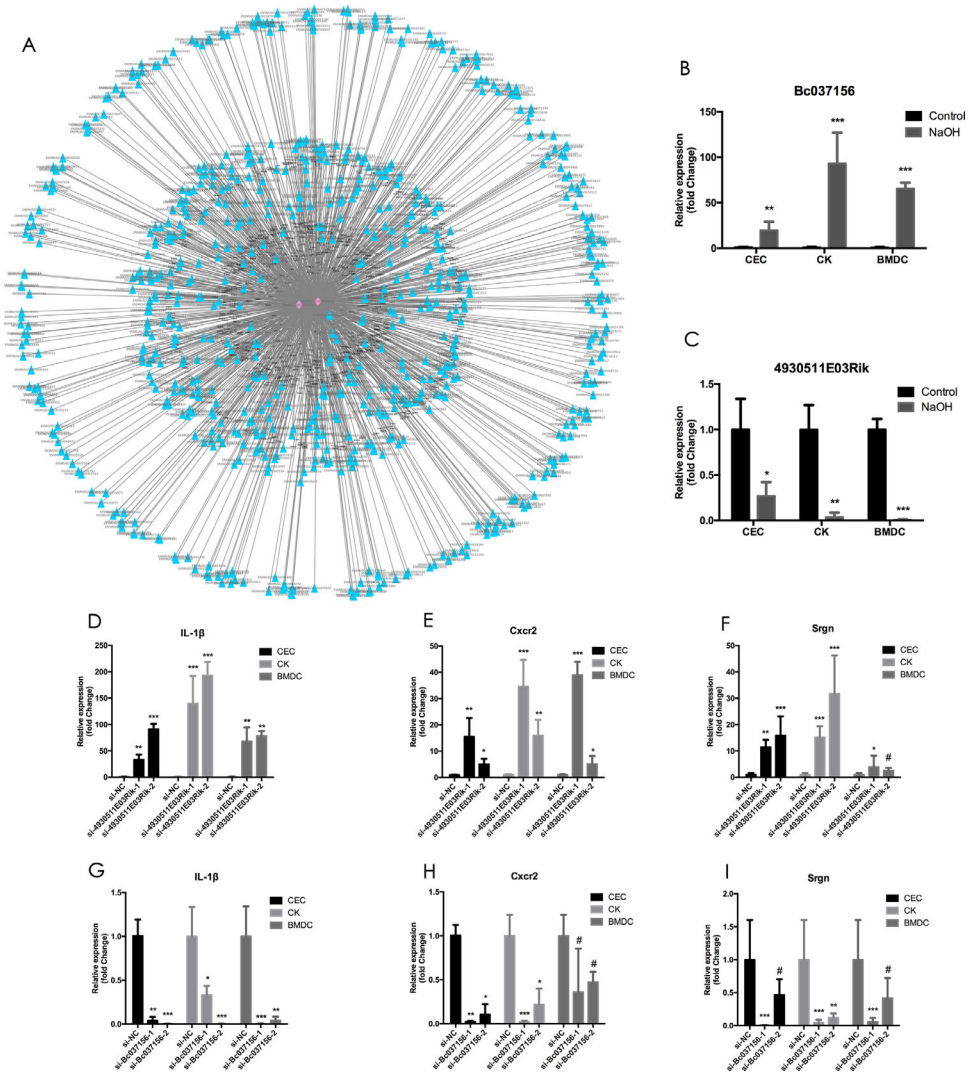

Figure 6. Validation of lncRNAs Bc037156 and 4930511E03Rik, regulating the potential target mRNAs in vivo. (**A**) The lncRNA-mRNA co-expression network of Bc037156 and 4930511E03Rik, and their regulated mRNAs. (**B, C**) The expression levels of Bc037156 and 4930511E03Rik in CEC, CK, and BMDC after NaOH treatment. (**D–F**) After transfection with si-4930511E03Rik, the mRNA levels of IL-1β, Cxcr2, and Srgn in CEC, CK, and BMDC following NaOH treatment. **D** to **F** After transfection with si- Bc037156, the mRNA levels of IL-1β, Cxcr2, and Srgn in CEC, CK, and BMDC following NaOH treatment. #: $P > 0.05$, *: $P < 0.05$, **: $P < 0.01$, ***: $P < 0.001$. CEC, corneal epithelial cell; CK, corneal keratocyte; BMDC, bone marrow dendritic cell; IL-1β, interleukin-1β; Cxcr2, CXC chemokine receptor 2; Srgn, serglycin.

CAB remains incompletely understood, warranting further exploration.

Increasing evidence has shown that lncRNAs participated in numerous biological process.[29] Huang et al. have performed lncRNAs microarrays analyses using an alkaline burn-induced CNV model, identifying 154 differentially expressed lncRNAs. These results suggested that lncRNAs were the potential regulators of CNV.[30] However, our results were not consistent with these previous findings. On reviewing their data, we observed that only 2 identified lncRNAs, A930006I01Rik and Gm2109, were consistent with our findings. It should be noted that the study by Huang et al. was published in 2015 and performed microarray analysis for 16,251 lncRNAs, identifying 154 differentially expressed lncRNAs. However, in the present study, we identified 4436 differentially expressed lncRNAs, a much larger number than that reported by Huang et al. Moreover, microarray analysis cannot determine a large number of potential lncRNAs and target mRNAs. We performed whole transcriptome sequencing and detected additional known and novel lncRNAs, finally identifying the most related lncRNAs. Hence, we speculated that the identified lncRNAs might be more credible than those that were presented in the study by Huang et al.

In the present study, 4436 aberrantly expressed lncRNAs were identified, notably, Bc037156 and 4930511E03Rik were verified as the potential regulated lncRNAs. The two lncRNAs are well-known lncRNAs. Bc037156 ENSMUSG00000105888 (lincRNA), located in chr5, was significantly upregulated. 4930511E03Rik ENSMUSG00000108187 (lincRNA), located in chr6, was significantly downregulated. Based on previous studies, Bai et al. selected[31] Neat1 may be a potential target for CNV as it is a key transcriptional regulator in cancer cell growth and inflammatory diseases. However,

they were unable to accurately identify the lncRNAs via sequencing. Nevertheless, they demonstrated that lncRNA Neat1 promotes an inflammatory response and induces CNV after an alkali burn.[31] In another study, they further reported that corneal angiogenesis is alleviated by regulating the lncRNA Neat1.[15] These results are consistent with our findings. However, we demonstrated that the expression level of Bc037156 was markedly higher than that of Neat1. Hence, Bc037156 and 4930511E03Rik were selected for subsequence research. To date, this is the first study to detect deferentially expressed lncRNAs in the CAB model using whole-genome sequencing. These novel lncRNAs provide a guide for future research and need to be comprehensively investigated to determine the functional role and regulatory mechanisms underlying the pathology of a CAB.

To explore signaling pathways and their relationship of biological systems, we performed GO and KEGG enrichment analyses. The results revealed that lncRNAs participate in cell process and biological regulation, cell part and organelle, catalytic activity, and binding. The pathway analysis demonstrated that MAPK signaling pathway was the most enriched, which is involved with cell proliferation, cell differentiation, and inflammation. In addition, the other signaling pathways, such as the TNF signaling pathway, VEGF signaling pathway, Th1 and Th2 cell differentiation, Th17 cell differentiation, the T cell receptor signaling pathway, PI3K-Akt signaling pathway, cytokine-cytokine receptor interaction, and MAPK signaling pathway were also enriched. Chen et al. have demonstrated that of MAPK-activated protein kinase 2 (MK2) activation selectively inhibited alkali induced corneal inflammation via p38/MAPK.[32] Furthermore, VEGF activates downstream PI3K-AKT-mTOR and Erk-MAPK signaling pathways to induce the transcription of angiogenesis-related genes.[33] Additionally, TNF, as a critical cytokine, can induce diverse intracellular signaling pathways, including apoptosis, cell survival, inflammation, and immunity. After stimulation of the cornea with an alkaline solution, the TNF signaling pathway is initiated. Reportedly, the anti-TNF-α antibody causes a marked reduction in CNV, protecting the retina and cornea from alkali damage.[34] Downstream of the TNF signaling pathway, the MAPK cascade is activated in response to pro-inflammatory stimuli. Furthermore, leukocytes are recruited and activated, promoting T cells, including Th1, Th2, and Th17 cell differentiation, and stimulating a strong cell-mediated immune response. Notably, modulating the balance between Th1/Th2 cell differentiation and cytokine production is crucial for immunity and host protection.

To further investigate the regulation between candidate lncRNAs and target mRNAs, we selected the top 13 aberrantly expressed mRNAs. The results of RT-qPCR validated that all selected genes were significantly and differentially expressed in the alkali-burned cornea when compared with the normal cornea. Combined with the lncRNA-mRNA co-expression network analysis, we revealed that both Bc037156 and 4930511E03Rik regulated Srgn, IL-1β, and Cxcr2. IL-1β is upregulated in multiple signaling pathways, such as MAPK and TNF, triggering downstream inflammation, and promoting T cell differentiation and activation. Cxcr2 is involved in the MAPK and cytokine-cytokine receptor interaction signaling pathway. Reportedly, an MK2 inhibitor suppressed IL-1β and IL-6 expression via the MAPK signaling pathway, resulting in reduced alkali burn-induced inflammation and inflammatory cell infiltration.[32] Addison et al. have detected that Cxcr2 played a functional role in angiogenesis.[35] Moreover, another research has revealed that Cxcr2 was critical to the extravasation of neutrophils into the avascular cornea.[36] In addition, we performed the experiments in vivo to verify the regulatory mechanism. The expression levels of IL-1β, Cxcr2, and Srgn after si-4930511E03Rik treatment were significantly elevated in the CEC, CK, and BMDC groups. Moreover, IL-1β and Srgn were significantly reduced following Bc037156 knockdown in all three cell types. In CEC and CK, expression levels of Cxcr2 were significantly reduced. These results confirmed that Bc037156 and 4930511E03Rik may regulate the target genes IL-1β, Cxcr2, and Srgn during the pathological process of a CAB.

In conclusion, our study was the first to demonstrate the lncRNA and mRNA high-transcriptome sequencing analysis of CAB. Based on the results, 4436 dysregulated lncRNAs were predicted. Among them, Bc037156 and 4930511E03Rik were verified as potentially regulated lncRNAs. Furthermore, Srgn, IL-1β, and Cxcr2 were regulated by Bc037156 and 4930511E03Rik, respectively, and may be involved in the pathological process of a CAB. Thus, our study provided a clue to understand the molecular machine and therapeutic targets based on the differential expressed lncRNAs and mRNAs.

Acknowledgments

The authors thank Bingqing Li for his guidance on bioinformatics data analysis.

Supported by the National Natural Science Foundation of China (No. 82060179, 82070982, 81760172, 81760178, 81660168, 81660161, 81560166), the Natural Science Foundation of Guangxi Zhuang Autonomous Region (No. 2020GXNSFBA159015, 2018GXNSFAA281128, 2018GXNSFAA050003, 桂科AD20297030), 139 Guangxi Training Program Foundation for the High-level Talents.

Disclosure: **L. Jiang,** None; **W. He,** None; **F. Tang,** None; **N. Tang,** None; **G. Huang,** None; **W. Huang,** None; **X. Wu,** None; **J. Guan,** None; **S. Zeng,** None; **M. Li,** None; **Q. Chen,** None; **M. Zhang,** None; **H. Zhong,** None; **Q. Lan,** None; **L. Cui,** None; **L. Li,** None; **F. Xu,** None

References

1. Bian F, Pelegrino FS, Henriksson JT, et al. Differential effects of dexamethasone and doxycycline on inflammation and MMP production in murine alkali-burned corneas associated with dry eye. *Ocul Surf*. 2016;14(2):242–254.
2. Pfister RR. The effects of chemical injury on the ocular surface. *Ophthalmology*. 1983;90(6):601–609.
3. Chang CY, Wang MC, Miyagawa T, et al. Preparation of arginine-glycine-aspartic acid-modified biopolymeric nanoparticles containing epigalloccatechin-3-gallate for targeting vascular endothelial cells to inhibit corneal neovascularization. *Int J Nanomedicine*. 2017;12:279–294.
4. Jiang L, Liu T, Xie L, Ouyang C, Ji J, Huang T. AICAR prolongs corneal allograft survival via the AMPK-mTOR signaling pathway in mice. *Biomed Pharmacother*. 2019;113:108558.
5. Estrella-Mendoza MF, Jimenez-Gomez F, Lopez-Ornelas A, Perez-Gutierrez RM, Flores-Estrada J. Cucurbita argyrosperma seed extracts attenuate angiogenesis in a corneal chemical burn model. *Nutrients*. 2019;11(5):1184.

6. Soiberman U, Kambhampati SP, Wu T, et al. Subconjunctival injectable dendrimer-dexamethasone gel for the treatment of corneal inflammation. *Biomaterials*. 2017;125:38–53.
7. Sharma N, Kaur M, Agarwal T, Sangwan VS, Vajpayee RB. Treatment of acute ocular chemical burns. *Surv Ophthalmol*. 2018;63(2):214–235.
8. Beermann J, Piccoli MT, Viereck J, Thum T. Non-coding RNAs in development and disease: background, mechanisms, and therapeutic approaches. *Physiol Rev*. 2016;96(4):1297–1325.
9. Rinn JL, Chang HY. Long noncoding RNAs: molecular modalities to organismal functions. *Annu Rev Biochem*. 2020;89:283–308.
10. Yao RW, Wang Y, Chen LL. Cellular functions of long noncoding RNAs. *Nat Cell Biol*. 2019;21(5):542–551.
11. Gil N, Ulitsky I. Regulation of gene expression by cis-acting long non-coding RNAs. *Nat Rev Genet*. 2020;21(2):102–117.
12. Lu D, Thum T. RNA-based diagnostic and therapeutic strategies for cardiovascular disease. *Nat Rev Cardiol*. 2019;16(11):661–674.
13. Leti F, Morrison E, DiStefano JK. Long noncoding RNAs in the pathogenesis of diabetic kidney disease: implications for novel therapeutic strategies. *Per Med*. 2017;14(3):271–278.
14. Sharma U, Barwal TS, Malhotra A, et al. Long non-coding RNA TINCR as potential biomarker and therapeutic target for cancer. *Life Sci*. 2020;257:118035.
15. Bai Y, Wang W, Zhang Y, Zhang F, Zhang H. lncRNA MIAT suppression alleviates corneal angiogenesis through regulating miR-1246/ACE. *Cell Cycle*. 2019;18(6-7):661–669.
16. Chen X, Guo W, Xu XJ, et al. Melanoma long non-coding RNA signature predicts prognostic survival and directs clinical risk-specific treatments. *J Dermatol Sci*. 2017;85(3):226–234.
17. Movahedan A, Afsharkhamseh N, Sagha HM, et al. Loss of Notch1 disrupts the barrier repair in the corneal epithelium. *PLoS One*. 2013;8(7):e69113.
18. Liu H, Gao W, Yuan J, et al. Exosomes derived from dendritic cells improve cardiac function via activation of CD4(+) T lymphocytes after myocardial infarction. *J Mol Cell Cardiol*. 2016;91:123–133.
19. Pertea M, Pertea GM, Antonescu CM, Chang TC, Mendell JT, Salzberg SL. StringTie enables improved reconstruction of a transcriptome from RNA-seq reads. *Nat Biotechnol*. 2015;33(3):290–295.
20. Mistry J, Bateman A, Finn RD. Predicting active site residue annotations in the Pfam database. *BMC Bioinformatics*. 2007;8:298.
21. Cabili MN, Trapnell C, Goff L, et al. Integrative annotation of human large intergenic noncoding RNAs reveals global properties and specific subclasses. *Genes Dev*. 2011;25(18):1915–1927.
22. Wang L, Feng Z, Wang X, Wang X, Zhang X. DEGseq: an R package for identifying differentially expressed genes from RNA-seq data. *Bioinformatics*. 2010;26(1):136–138.
23. Abdelfattah NS, Amgad M, Zayed AA. Host immune cellular reactions in corneal neovascularization. *Int J Ophthalmol*. 2016;9(4):625–633.
24. Mochimaru H, Usui T, Yaguchi T, et al. Suppression of alkali burn-induced corneal neovascularization by dendritic cell vaccination targeting VEGF receptor 2. *Invest Ophthalmol Vis Sci*. 2008;49(5):2172–2177.
25. Bakunowicz-Lazarczyk A, Urban B. Assessment of therapeutic options for reducing alkali burn-induced corneal neovascularization and inflammation. *Adv Med Sci*. 2016;61(1):101–112.
26. Wu Y, Xu Z, Yang Y, et al. Tetramethylpyrazine (TMP) ameliorates corneal neovascularization via regulating cell infiltration into cornea after alkali burn. *Biomed Pharmacother*. 2019;109:1041–1051.
27. Xu W, Liu K, Li T, et al. An in situ hydrogel based on carboxymethyl chitosan and sodium alginate dialdehyde for corneal wound healing after alkali burn. *J Biomed Mater Res A*. 2019;107(4):742–754.
28. Arima T, Uchiyama M, Nakano Y, et al. Peroxisome proliferator-activated receptor alpha agonist suppresses neovascularization by reducing both vascular endothelial growth factor and angiopoietin-2 in corneal alkali burn. *Sci Rep*. 2017;7(1):17763.
29. Cisse Y, Bai L, Chen MT. LncRNAs in ocular neovascularizations. *Int J Ophthalmol*. 2019;12(12):1959–1965.
30. Huang J, Li YJ, Liu JY, et al. Identification of corneal neovascularization-related long noncoding RNAs through microarray analysis. *Cornea*. 2015;34(5):580–587.
31. Bai YH, Lv Y, Wang WQ, Sun GL, Zhang HH. LncRNA NEAT1 promotes inflammatory response and induces corneal neovascularization. *J Mol Endocrinol*. 2018;61(4):231–239.
32. Chen Y, Yang W, Zhang X, et al. MK2 inhibitor reduces alkali burn-induced inflammation in rat cornea. *Sci Rep*. 2016;6:28145.
33. Sun J, Huang W, Yang SF, et al. Galphai1 and Galphai3mediate VEGF-induced VEGFR2 endocytosis, signaling and angiogenesis. *Theranostics*. 2018;8(17):4695–4709.
34. Cade F, Paschalis EI, Regatieri CV, Vavvas DG, Dana R, Dohlman CH. Alkali burn to the eye: protection using TNF-alpha inhibition. *Cornea*. 2014;33(4):382–389.
35. Addison CL, Daniel TO, Burdick MD, et al. The CXC chemokine receptor 2, CXCR2, is the putative receptor for ELR+ CXC chemokine-induced angiogenic activity. *J Immunol*. 2000;165(9):5269–5277.
36. Khan S, Cole N, Hume EB, et al. The role of CXC chemokine receptor 2 in Pseudomonas aeruginosa corneal infection. *J Leukoc Biol*. 2007;81(1):315–318.

Investigative Ophthalmology & Visual Science